Powder Technology 336 (2018) 273–281

Contents lists available at ScienceDirect

Powder Technology

journal homepage: www.elsevier.com/locate/powtec

Measuring attrition properties of calcium looping materials in a 30 kW pilot plant

Mónica Alonso [a,*], Borja Arias [a], José Ramón Fernández [a], Olivier Bughin [b], Carlos Abanades [a]

[a] Instituto Nacional del Carbón, CSIC-INCAR, Francisco Pintado Fe, 26, 33011 Oviedo, Spain
[b] Carmeuse Research & Technology, Rue du Château 13A, 5300 Seilles, Belgium

ARTICLE INFO

Article history:
Received 26 October 2017
Received in revised form 28 May 2018
Accepted 4 June 2018
Available online 6 June 2018

Keywords:
Limestone
Attrition
Calcium looping
Circulating fluidized bed
CO_2 capture

ABSTRACT

The attrition of CaO-based solids operating in calcium looping (CaL) post-combustion CO_2 capture systems is an important factor to consider when limestones are selected as sorbent precursors. In this work, four commercial natural limestones with similar chemical compositions but with very different mechanical properties were tested in a 30kWth calcium looping pilot plant. The main attrition mechanisms that act upon the limestones (i.e. fragmentation, decrepitation and abrasion) were identified on the basis of the evolution of their particle size distributions during the start-up and the first calcination of each batch. Great differences in the performance of the selected limestones were observed, which confirms the suitability of the experimental procedure employed for sorbent screening purposes in these high-velocity, high-temperature pilot plants. Several attrition indexes reported in the literature were tested to conclude that the Total Particle Generated Index (TPGI) and the Maximum Diameter of Particles Generated (MDPG) indexes are the most useful for quantifying attrition phenomena and rank limestones.

1. Introduction

Calcium looping, CaL, is an emerging CO_2 capture technology in which particles of CaO are used to capture CO_2 from a flue gas, typically in a fluidized bed, giving rise to $CaCO_3$, which is subsequently decomposed in an oxy-fired fluidized bed combustor [1–7]. The calcium looping in fluidized beds for post-combustion applications has already been demonstrated in several test facilities of up to 1–2 MW_{th} scale [8–12]. The rapid development of the CaL technology is due to the use of reactor configurations and materials very similar to those typically employed in large-scale fluidized-bed combustion power plants.. In CaL systems, natural limestone is used as a source of CaO because of its low cost and suitable fluidisation properties. An important design parameter of the calcium looping processes is the consumption of limestone (i. e., the make-up flow) needed to sustain a certain level of activity of the CaO material for the capture of CO_2 and to compensate for the CaO loss in the cyclones located downstream of the interconnected carbonator and calciner reactors. Thus, to ensure the selection of the most appropriate sorbent the mechanical properties of the material circulating between the reactors must be taken into consideration.

Attrition, defined as the unwanted breakage of particles, results in the degradation of the solids and in a change in the size and number of particles. It is influenced by a large number of variables related to the design of the system the properties of the solids and the reacting environment [13]. In fluidized beds the most common attrition mechanisms are induced by mechanical motion and by temperature or pressure gradients inside the particles as they are subjected to fast changes in their environment [14, 15]. The main attrition mechanisms caused by mechanical motion are abrasion, when breakage takes place exclusively on the particle surface generating fines, and fragmentation, when the particles are broken into similar coarse fragments [13, 16]. Abrasion usually takes place due to the low velocity impacts between particles in the dense bed. There is an initial peak of fines generation which then decreases as the particles round off [17–19]. Fragmentation typically occurs due to high velocity impacts in the grid jets, cyclones and at the exit of the circulating fluidized bed reactors. The extent of particle fragmentation increases with the impact velocity, the multiplicity of impacts and it is also affected by the specific properties of the solids [20]. On the other hand, the main attrition mechanism induced by internal forces is decrepitation (or primary fragmentation), which generates both coarse and fine particles. This phenomenon is generally caused by thermal shock during rapid heating and/or by the fast release of gas from the solids [13].

There is substantial literature available on the attrition of limestone in fluidized bed combustors, where CaO is typically used as a SO_2 sorbent [21–26]. However, the knowledge acquired so far on this phenomenon for the specific conditions of post-combustion CaL systems is still scarce [7, 20, 27–34]. There is general agreement that CaO-based sorbents sinter and deactivate during the CO_2 capture process (i.e. their

* Corresponding author.
E-mail address: mac@incar.csic.es (M. Alonso).

https://doi.org/10.1016/j.powtec.2018.06.011

CO_2 carrying capacity diminishes as the number of carbonation-calcination cycles increases) and they become progressively harder and rounder in shape [27, 28, 30–34]. The sulfation of CaO greatly reduces the generation of fines from abrasion, since the sulfate layer formed on the outer surface tends to improve the strength of the particles [35, 36]. Moreover, calcination and carbonation reactions also affect the extension and pattern of fragmentation. The particles of raw limestones and re carbonated sorbents are the most resistant to impact loading, whereas those of calcined sorbents are the weakest [20]. Decrepitation in limestones is mainly caused by the release of CO_2 during the first calcination, which changes the morphology of particles, rather than by thermal shock [35].

Despite the existing consensus on the qualitative attrition mechanisms noted above, there is a wide variety of tests and techniques that are used to quantify attrition and to rank materials in terms of attrition performance. Standard attrition tests available for other applications do not provide sufficient relevant information for each type of material and application. The great variability in attrition of natural limestones requires for highly empirical approaches to investigate these phenomena under specific process conditions. No feasible method to study the different attrition mechanisms separately is available as yet (unlike the study of chemical reaction phenomena). Hence the use of lump attrition parameters like the "attrition index" is the norm in quantitative attrition studies.

The attrition index proposed by Forsythe and Hertwig in 1949 for fluid cracking catalysts [37] is still considered to be a useful parameter for evaluating solids mechanical degradation during fluidization. In this methodology, an attrition rate is arbitrary defined considering the amount of material with a particle size of below 44 μm (325 mesh) produced per hour. This index is useful for the comparative testing of materials under similar and strictly controlled conditions [13]. Other attrition indexes reported in the literature are based on Gwyn's formulation [38]. Gwyn assumes that the amount of material elutriated corresponds to the attrited material, which can be fitted to a power-law time dependent function. However, this formulation is only valid when abrasion is the main attrition mechanism during the operation. Some authors consider that these definitions are not sufficiently accurate for describing the attrition process since they do not take into account the breaking of particles when fines are not produced [16] or the fact that not all the fines produced are elutriated [39]. Amblard et al. [39] recently defined another attrition index to overcome these limitations. This index is based on the evolution with time of the entire particle size distribution (PSD) of the solids during the test including the elutriated material (and not only the fines generated below 45 μm, as in the case of classical attrition indexes). The main limitation of this procedure is the greater experimental effort needed to obtain a detailed assessment of the particle size distributions under realistic conditions.

In the present work, the methodology developed by Amblard et al. [39],has been adapted to study the resistance to attrition of four limestones with similar chemical composition in a 30 kW fluidized-bed pilot plant operated under conditions similar to those of larger calcium looping systems (i.e., with high gas velocities and high temperatures). With this procedure, the dominant attrition mechanisms for each limestone are identified and the solids can be ranked according to the extent of particle attrition, which can facilitate the screening of sorbents in calcium looping applications.

2. Experimental

2.1. Limestones

Four commercial limestones, labelled A, B, C and D, were used for the purpose of this study. The materials were provided by Carmeuse from their extensive database of limestones with different mechanical properties and geological origin. The chemical compositions of these limestones were determined by means of an X-Ray Fluorescence Spectrometer (SRS 3000 Bruker) following the fused cast-bead method (PERLX'3 Philips). As can be seen in Table 1, from a chemical composition point of view, all the limestones are of a high purity, although it should be noted that limestone B has a higher SiO_2 content.

Carbonation-calcination tests were carried out in order to determine the CO_2 carrying capacity. The experiments were performed in a thermogravimetric analyser that has been described in detail elsewhere [40]. Fig. 1 shows the evolution of the maximum carbonation conversion (X_N) for the four sorbents with the number of carbonation-calcination cycles. It is generally accepted that the decay in the CO_2 carrying capacity for a variety of limes and reaction conditions can be expressed by Eq. 1, employing an average deactivation constant k of 0.52 and a residual molar conversion X_r of 0.075 [41].

$$X_N = \frac{1}{\frac{1}{(1-X_r)} + kN} + X_r \quad (1)$$

As can be seen in Fig. 1, the deactivation curves of the four sorbents are very similar and follow the trend marked by Eq. (1).

Moreover, the Particle Size Distributions (PSDs) of the fresh limestones were obtained using a Beckman-Coulter LS 13320 laser diffraction particle size analyser in dry mode. Air was used to disperse the solids in the laser chamber. In accordance with the recommendations of the manufacturer, 1 wt% of fumed silica ($d_p = 7$ nm) was added to facilitate the dispersion of the samples.

As can be seen in Fig. 2, the fresh A-D limestones have similar PSDs and in all cases around 90 vol% of the distributions are between 100 and 400 μm. Therefore, the starting point for all the attrition test is a group of limestones with almost identical particle size distributions and chemical performance as CO_2 regenerable sorbents.

2.2. The 30 kW CaL pilot plant at INCAR-CSIC

Although the outline of the 30 kW plant has been explained in detail elsewhere [42–44], a brief description of the pilot plant is given below, including the modifications made for the attrition test. The test rig consists of two circulating fluidized bed reactors (see Fig. 3). Both reactors have an internal diameter of 0.1 m. The carbonator is 6.3 m in height, whereas the calciner has a height of 6.1 m. There are no air distributors in the reactors to facilitate the feed of solids directly to the risers. The solids are fed in by means of two screw-feeders located at the cold air entrances to the risers. The air is blown into the facility by a fan and the flowrates to the risers and loop-seals are independently controlled by means of mass flow controllers. The bottom 3 m of each riser is surrounded by independently controlled electrical ovens, while the rest of the primary loop is thermally insulated. Each riser is connected to a high-efficiency primary cyclone, where the solids and gas phases are separated with a efficiency of about 97–99%. There are also two secondary cyclones before the stacks to ensure that there is no significant loss of solids from the facility. Downstream of the primary cyclones, the solids fall into the loop-seals through the standpipes. The loop-

Table 1
XRF analysis of the limestones (in wt%).

Oxide	A	B	C	D
MgO	0.37	0.85	0.65	0.48
Al_2O_3	0.00	0.27	0.13	0.18
SiO_2	0.18	1.40	0.3	0.56
SrO	0.00	0.02	0.02	0.03
K_2O	0.00	0.05	0.00	0.03
CaO	55.92	54.14	55.64	55.21
Fe_2O_3	0.00	0.00	0.05	0.00
SO_3	0.07	0.21	0.00	0.10
LOI[a]	43.46	43.05	43.35	43.44
Total	100.00	99.99	100.14	100.03

[a] LOI: Lost On Ignition.

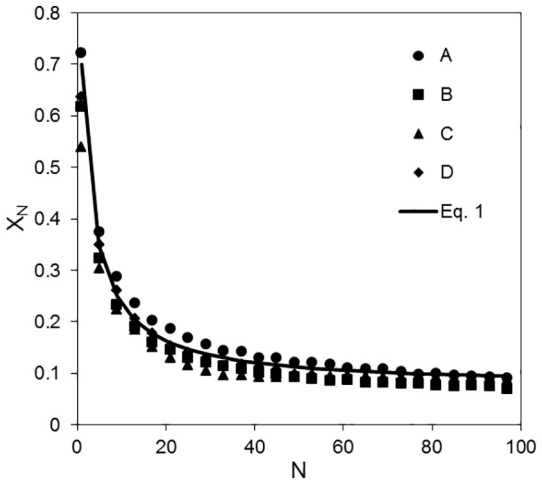

Fig. 1. Evolution of the maximum CO_2 carrying capacity of four sorbents with the number of carbonation-calcination cycles and comparison with eq. 1 at average parameter values (calcination stage carried out at 900 °C for 10 min in air; carbonation stage carried out at 650 °C for 10 min with 10 vol% CO_2 in air).

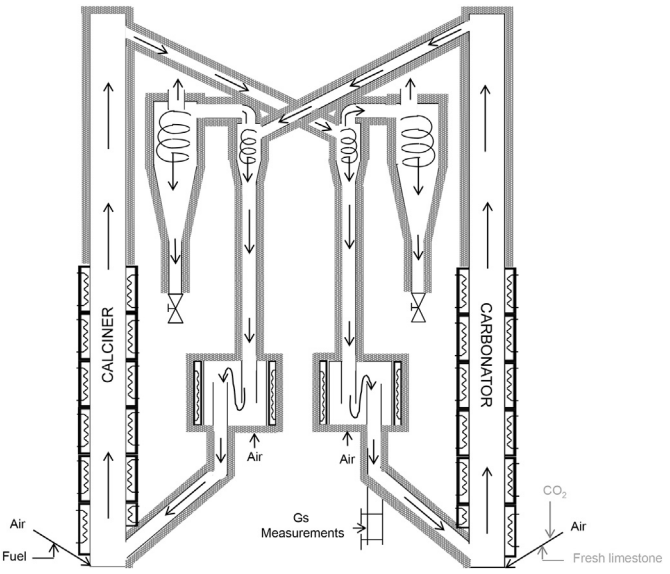

Fig. 3. Schematics of the 30 kW pilot plant at INCAR-CSIC. Grey lines and symbols are used only for carbonation/calcination tests.

seals are fluidized by air that comes through gas distributors. The solids flow into the opposite riser through diplegs, fitted with small quartz windows so that the solids circulation can be visually checked. Furthermore, in the dipleg leading to the carbonator, a by-pass is located just below the loop-seal to allow the solids circulation flowrates (G_s) to be measured and solid samples to be extracted (see Fig. 3). The solids circulation rate is measured by diverting the solids stream to a dead volume between two valves for a certain period of time.

The test facility is equipped with 40 thermocouples, seven of which are fitted in each riser, 22 in the primary loop and four around the secondary cyclones. Twenty differential pressure taps and four zirconia oxygen probes have been installed in the carbonator and in the calciner. There are also two on-line gas analysers for measuring the concentrations of CO, CO_2 and O_2.

2.3. Procedures

2.3.1. Pilot plant tests

The attrition tests started by distributing a batch of fresh limestone of around 20 kg between the carbonator and calciner (roughly 50% each). Air was fed to the facility when the temperature in the ovens reached 400 °C. From this point on, the air mass flowrates were kept constant at 15 Nm^3/h in each riser and at 4 Nm^3/h in each loop-seal. Once the temperature had reached around 550 °C at the exit of the risers, the secondary cyclones were emptied of solids and their weight and samples were recorded. In these initial conditions, the facility was operated at low solids circulation rates (<0.5 kg/m^2 s). Then, coal was fed at a rate of 1.5 kg/h into the calciner, which allowed the average temperature of reactor to be kept below 780 °C during at least 1 h. At this point, the calcination conversion of the initial batch of limestone was still very low (<10%), which means that any attrition in the initial batch would have been caused mainly by mechanical forces related to the circulation of the solids in the system. Then, solids samples from the risers and the emptied secondary cyclones were taken and the solids circulation flowrate was measured. The coal feed rate was subsequently increased to the maximum value allowable in order to carry out the combustion with an excess of air of around 5%. Meanwhile, the electric ovens were set to maximum power in order to calcine the batch of limestone as fast as possible. Subsequently, after every 15–20 min, solid samples of about 10 g were taken from the risers for PSD analysis, the secondary cyclones were emptied and the accumulated solids were weighed. The solids circulation flowrate was measured at the same frequency. At that time, around 500 g were extracted in order to clean the pipe between the by-pass and the first valve. Subsequently, these solids were returned to the system. In contrast, the solids collected in the secondary cyclones were not returned during the tests. As the primary cyclones are of high-efficiency, the amount of solids extracted from the

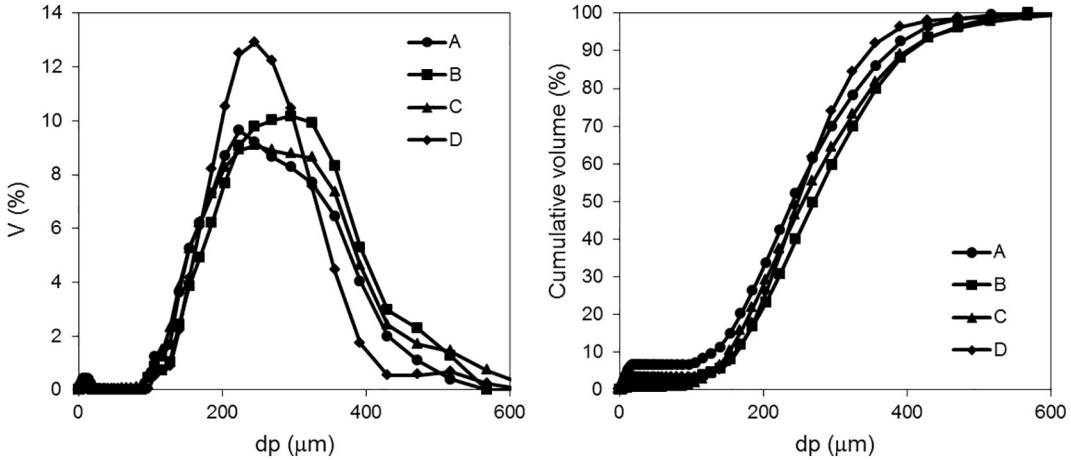

Fig. 2. Left. Particle Size Distribution for the fresh limestones. Right. Cumulative curve.

secondary cyclones was very low in comparison with the total mass of solids present in the system. Between 10 and 50 g were collected each time the cyclones were emptied. Moreover, there was not addition of fresh limestone during the tests in order to avoid any alteration in the evolution of the Particle Size Distributions. CO_2 was not fed into the carbonator, since the re-carbonation of the particles would lead to a lower degree of attrition [20]. The carbon and sulphur contents in all the solid samples were measured by a 230 CS LECO analyser to allow the closure of the carbon mass balances. In order to avoid temperature excursions in the calciner when the batch of limestone approached total calcination, each experiment was considered to be finished when the average carbon concentration measured in these samples was lower than 3 wt% (i.e., a $CaCO_3$ molar fraction lower than 15%). The particle size distribution of selected samples from the experiments was determined by means of a laser diffraction particle size analyser. Finally, at the end of each experiment, the solids accumulated in the primary loop (i. e., in risers, loop-seals and circulation bypass) were extracted separately and weighed in order to close the global mass balances of the experiments. Only those tests in which the global solid mass balance closure was higher than 90% were taken into account.

2.3.2. Calculation of the attrition indexes

The Attrition Rate based on the Forsythe and Hertwig formulation [37] was estimated as follows:

$$\text{Attrition Rate } (AR, \%/h) = \frac{\Delta V_{cum,t}}{\Delta t} \tag{2}$$

where $\Delta V_{cum,t}$ is the cumulative volume (%) below 45 μm after a certain period of time Δt (expressed in hours). This index requires the re-construction of the entire particle size distribution at a chosen time and the main limitation is that the attrition calculated is only associated with the change in the fraction below 45 μm.

Another index considered in this work is the Attrition Index (m) based on Gwyn's formulation [38]:

$$-\ln W_{elutriated} = \gamma - m\ lnt \tag{3}$$

where γ refers to the severity of the attrition conditions and to the initial particle size distribution. In this case, it is assumed that all attrited material has been elutriated from the system. The main advantage of this index is that no PSDs are required, which facilitates its calculation. Moreover, it is the basis for the Air Jet Index (AJI) in the ASTM D-5757 [13].

Amblard et al. [39] defined more recently the Total Particle Generation Index (TPGI). This parameter can be calculated from the sinusoidal-type curve obtained from the difference between the particle size distribution (PSD) curve of a sample and a reference particle size distribution, which usually corresponds to the PSD curve measured before the attrition test. The positive area under the difference curve corresponds to the amount of particles that have been generated by attrition (i.e., the Total Particle Generating Index), whereas the negative area is related to the amount of particles that have suffered attrition. Moreover, the point where the difference curve cuts the X-axis (i.e., particle diameter in a PSD) indicates the Maximum Diameter of Particles Generated (MDPG) by attrition. The calculation of the Total Particle Generation Index entails the reconstruction of the particle size distribution of the whole batch of material initially loaded at any selected time. The solid mass balance includes the mass of solids that have been elutriated into the secondary cyclones as well as the composition of the samples from the primary loop. First, the weight fraction of the initial batch of solids that remains in the primary loop at a certain time, t, is defined as:

$$w_{loop} = 1 - \frac{(m_{2CB} + m_{2CC})}{(m_0 - m_{CO2,calc})} = 1 - \frac{(m_{2CB} + m_{2CC})}{m_0\left(\frac{56}{100} + \frac{44}{100}\frac{w_{C,ave}}{w_{C,0}}\right)} \tag{4}$$

where m_i are the cumulative weights of the solids from the secondary cyclone of the carbonator (2CB), the secondary cyclone of the calciner (2CC), and the weight of the CO_2 evolved from calcination (CO_2,calc). The CO_2 released from calcination is obtained from the mass balance on the gas phase taking into account the concentration of CO_2 measured by the analyzers and the combustion mass balance in the calciner. The $w_{C,ave}$ is the average carbon weight fraction measured by the LECO analyser of the solid samples extracted from the primary loop (i.e. carbonator, calciner and circulation). Both m_0 and $w_{C,0}$ refer to the initial weight of fresh limestone in the experiment and the carbon content of the fresh limestone, respectively. Similarly, the mass fraction of solids that has left the loop through each secondary cyclone is calculated as follows:

$$w_{2CB} = \frac{m_{2CB}}{(m_0 - m_{CO2,calc})} = \frac{m_{2CB}}{m_0\left(\frac{56}{100} + \frac{44}{100}\frac{w_{C,ave}}{w_{C,0}}\right)} \tag{5}$$

$$w_{2CC} = \frac{m_{2CC}}{(m_0 - m_{CO2,calc})} = \frac{m_{2CC}}{m_0\left(\frac{56}{100} + \frac{44}{100}\frac{w_{C,ave}}{w_{C,0}}\right)} \tag{6}$$

Once these mass fractions are defined, the re-constructed PSD of the whole bed in the system at a certain time can be calculated thus:

$$PSD_t = w_{loop,t} \times PSD_{LOOP,t} + w_{2CB,t} \times PSD_{2CB,t} + w_{2CC,t} \times PSD_{2CC,t} \tag{7}$$

The Total Particle Generated Index (TPGI) can be calculated as follows:

$$TPGI\ (\%) = \sum_{dp=0}^{dp=MDPG} (PSD_t - PSD_0) \tag{8}$$

where PSD_0 is the Particle Size Distribution of the fresh limestone in differential form.

3. Results and discussion

From the evolution with time of the particle size distributions, represented in Fig. 4 for all the limestones considered in this work, it is possible to follow the trend of attrition phenomena.. During an attrition experiment, the cumulative PSD_t calculated by means of Eqs. (4)–(8) should always move with time towards the left-hand side of the initial PSD (at $t = 0$). However, as can be seen in Fig. 4, these movements were quantitatively for each limestone, as indicated by the differences in PSDs at similar experimental times. Limestone D showed the highest degree of attrition during the tests, since most of the particles after 5 h of operation had diameters below 200 μm. In contrast, limestone A exhibited the lowest degree of attrition, whereas limestones B and C exhibited intermediate particle breakage.

During the first 2.1 h of operation, the temperatures achieved in the reactors were sufficiently low to prevent limestone calcination, so the decrepitation phenomenon was negligible. The main mechanism of attrition during this period of time in limestones A, B and C was fragmentation, because the higher changes observed in the PSD curves corresponded to the larger particle sizes (200–600 μm) and the fractions of particles lower than 100 μm only increased 6% compared with the initial PSD. In contrast, the abrasion phenomenon was prominent in Limestone D, since the fraction of particles larger than 430 μm disappeared after only 1.3 h while the fraction of particles smaller than 100 μm had increased to 10% after 2.1 h.

For longer operation times, the temperature achieved in the reactors was sufficiently high to favour the calcination of every limestone, so that the decrepitation mechanism caused significant changes in the PSD curves, especially in the period of time where the calcination achieved its maximum rate (i. e., calcination rates of about 0.02 mol CO_2/s). In

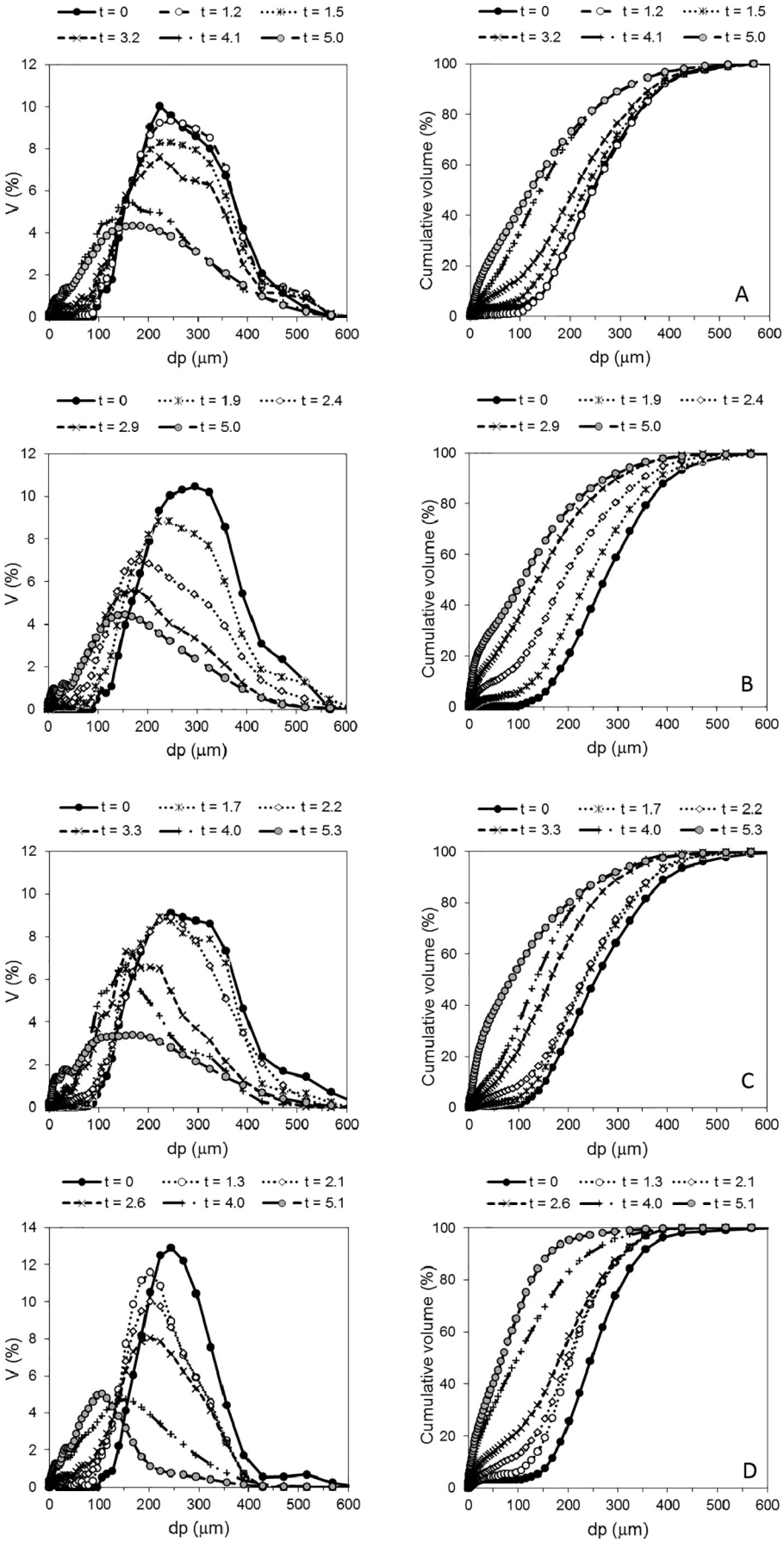

Fig. 4. Evolution with time of the Particle Size Distributions of limestones A-D obtained from the 30 kW pilot plant.

the case of limestone A, this period was between 3.2 and 4.1 h of the experimental time. The highest attrition corresponded to particles with sizes larger than 154 μm, while the fraction of particles below 100 μm increased from 16% to 35%. In the case of limestone B, the period of highest calcination rate was between 1.9 h and 2.9 h. Attrition mainly affected the fraction of particles with diameters larger than 154 μm while the fraction of particles smaller than 100 μm increased from 5% to 37%. For limestone C, this period of time occurred between 2.2 h and 3.3 h, where attrition acted mainly on particles larger than 185 μm and the fraction of particles with sizes smaller than 100 μm increased from 8.3% to 31%. Finally, for limestone D the maximum calcination rate was observed between 2.6 h and 4 h. During this period of time the particles most affected by attrition were those larger than 130 μm and the fraction of particles smaller than 100 μm increased from 21% to 49%. These data indicate that the production of fines due to decrepitation was higher in limestones B and D than in limestones A and C.

During the last part of the operation (between 1 h and 2 h depending on the test), attrition affected both the limestones and their counterpart limes as the molar fraction of calcium carbonate was lower than 0.5. In this period, the attrition of limestones A and B was mainly due to fragmentation as the production of particles with sizes smaller than 100 μm was around 5% in an hour. Meanwhile, in the case of limestones C and D the production of fines resulting from abrasion or decrepitation was substantial, since the fraction of particles smaller than 100 μm increased >10%. At the end of the tests, limestone A showed the highest average diameter (i.e. d_{50} of 128 μm) and had the lowest fraction of particles below 100 μm (41%). Limestone D showed the lowest average diameter (i.e., d_{50} of 68 μm) and the highest fraction of particles below 100 μm (65%). Limestones B and C exhibited intermediate values (i. e., d_{50} of 109 and 85 μm, and fractions of particles below 100 μm of 46% and 54% respectively).

The experimental data obtained from the pilot plant tests were used to calculate the different attrition indexes explained above, in order to rank the limestones A-D. First, the Attrition Index defined by Gwyn was calculated for every limestone by using Eq. (3). The results are represented in Fig. 5.

The slopes of the log-log elutriation weight vs. time shown in Fig. 5 indicate that limestone A presented the lowest Attrition Index, and therefore, the highest resistance to attrition, followed by limestone D, then limestone B and finally limestone C. This ranking coincides with the order in which the tests were carried out in the pilot plant. A decrease in the efficiency of the primary cyclone of the calciner was observed with each test due to the growing deposit of solids. This anomalous operation caused a gradual increase in the elutriation rates of the particles that had not actually suffered attrition. Under these conditions, the Attrition Index defined by Gwyn is not able to describe accurately the attrition phenomena and the changes observed in the PSD during the operation (as represented in Fig. 4).

The Attrition Rate index defined by Forsythe and Hertwig [37] was also estimated through Eq. (2) in order to represent more accurately the evolution of the attrition of the different limestones. As can be seen in Fig. 6, after 2 h of operation (without calcination) the Attrition Rates of limestones B, C and D were similar (i.e., 2.4%/h). In contrast, limestone A exhibited the lowest Attrition Rate (i.e. 0.8%/h) during this period. However, with the start of the calcination, the Attrition Rate of limestones B, C and D increased more sharply than limestone A. Decrepitation was probably the main attrition mechanism that generated fines during this period in these limestones. Coinciding with the maximum calcination rate (approximately between 2 h and 3 h for limestones B and C, and between 3 h and 4 h for limestones A and D), limestones A and B increased their Attrition Rate (up to 5.3%/h and 16.7%/h, respectively), whereas the attrition rates of limestones C and D decreased slightly. After this period, the attrition rates of limestones B and D decreased to values between 6 and 8%/h, respectively, whereas the attrition rate of limestones A and C increased to values of 11.4%/h and 17.5%/h, respectively. These tendencies suggest that in the case of limestone A abrasion or decrepitation with the production of fines were not as great as for the other limestones, although abrasion of its counterpart lime was significant. In the case of limestone B, fines were mainly caused by decrepitation, whereas abrasion had a smaller effect on the limestone and its counterpart lime. Limestone C was affected by abrasion and decrepitation increased the production rate of fines although less than for limestone B. However, its counterpart lime suffered a higher degree of abrasion than any other lime. Limestone D was the most affected by abrasion during solids circulation and during the initial period of calcination. However, the production of fines decreased at its maximum calcination rate and the effect of abrasion on its counterpart lime was not as large as before.

Finally, after 5 h of operation, limestones B and D showed the lowest attrition rates (i.e., 5.5%/h and 7.5%/h, respectively) with a downward trend for longer periods of time. In contrast, limestones C and A exhibited the highest attrition rates (i.e., 11.4%/h and 17.5%/h, respectively) after 5 h, and a tendency to increase.

On the basis of the index defined by Forsythe and Hertwig, limestones B and D ought to show the highest resistance to attrition, despite suffering great attrition rates between 2.5 h and 4.5 h once the experiments started. The weakest limestone would then be limestone C because its attrition rate increased with time more rapidly than that of the others, especially after 4.5 h of operation. However, these results do not show the changes observed in the PSD curves represented in Fig. 4.

Finally, the Total Particle Generation Index (TPGI) defined by Amblard et al. [39] was also calculated through Eq. (8) to obtain a better

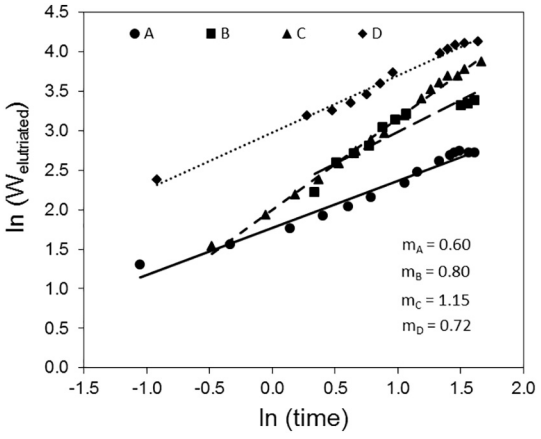

Fig. 5. Evolution with time of Attrition Index defined by Gwyn for all limestones in the 30 kW pilot plant.

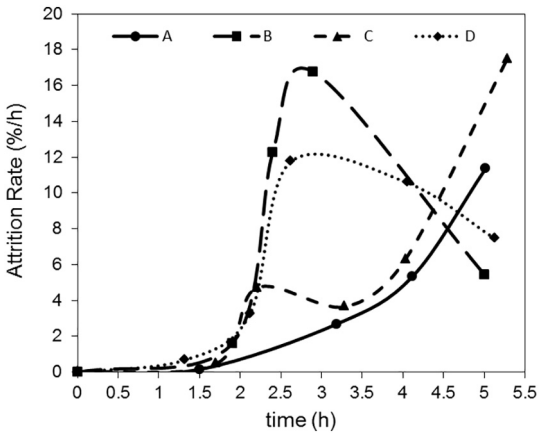

Fig. 6. Evolution with time of the Attrition Rate for all the limestones in the 30 kW pilot plant.

description of the attrition phenomena of the limestones studied in this work. Fig. 7 shows the curves obtained after subtracting the PSDs at different times from the initial PSD of each limestone. With this methodology, the differences between the limestones become more evident. As can be seen, the largest negative areas were obtained in the case of limestone D, which confirms that this material suffered the highest degree of attrition. In contrast, the smallest negative areas corresponded to limestone A, indicating that this solid exhibited the highest resistance to attrition, with limestones B and C showing an intermediate attrition behaviour.

The evolution with time of the TPGI and the Maximum Diameter of Particles Generated (MDPG) by attrition are depicted in Fig. 8 for all the limestones. During the first 2 h (i.e., without calcination), similar TPGIs were obtained for both limestones A and C, which means that both materials underwent a similar degree of attrition. A slightly higher TPGI were calculated for limestone B, whereas a TPGI almost three times higher was obtained for limestone D, which demonstrates that this material is the least resistant to attrition. During the same period of time, there was a dramatic decrease in the MDPGs for limestones A, B and C that can be attributed to the fragmentation mechanism. However, the fall in the MDPG in the case of limestone D was significantly lower, indicating that the abrasion mechanism must have been playing a considerable role, as this mechanism would cause very little changes in the MDPG. During the period of maximum calcination (i.e. between 2 and 3 h), limestone B showed the largest increase in the TPGI (i.e., of about 37%) and the largest fall in the MDPG, indicating that decrepitation in this material produced larger fragments than in any other limestone. On the other hand, the increase in the TPGI and the decrease in the MDPG for limestones A and C were similar, so it is safe to assume that it was the decrepitation mechanism of both limestones that mainly produced the fine particles. In the case of limestone D, the evolution of the TPGI and the MDPG followed similar trends to those measured previously without calcination, which means that decrepitation mechanism in this solid produced both fine and coarse fragments.

After this period of maximum calcination, the increase in TPGI in limestones A and B was similar (i.e. 3%/h) whereas limestone D showed the highest rate (17%/h) and limestone C an intermediate rate (i.e. 11%/h). The change in the MDPG was similar for limestones A, B and D (i.e., at around 10 μm per hour) indicating that fragmentation was not as determinant as in previous periods. However, the change in the MDPG of limestone C indicated that fragmentation still played an important role. Finally, after 5 h of operation, limestone A showed the lowest TPGI (i.e. 49%), limestones B and C similar values (61 and 60%, respectively), and limestone D exhibited the highest value (i.e., 81%).

On the basis of these results, the limestones can be ranked as follows. Limestone A is the most resistant to attrition as its TPGI and the change in the MDPG are the lowest after 5 h. In contrast, Limestone D is the least resistant due to the fact that its TPGI after 5 h is the highest. Although limestone B and limestone C have similar TPGI after 5 h, the change in the MDPG is higher in the case of limestone C, making B more preferable for use in the system than C. In view of these results, it is clear that the attrition indexes that best describe the changes in the PSDs shown in

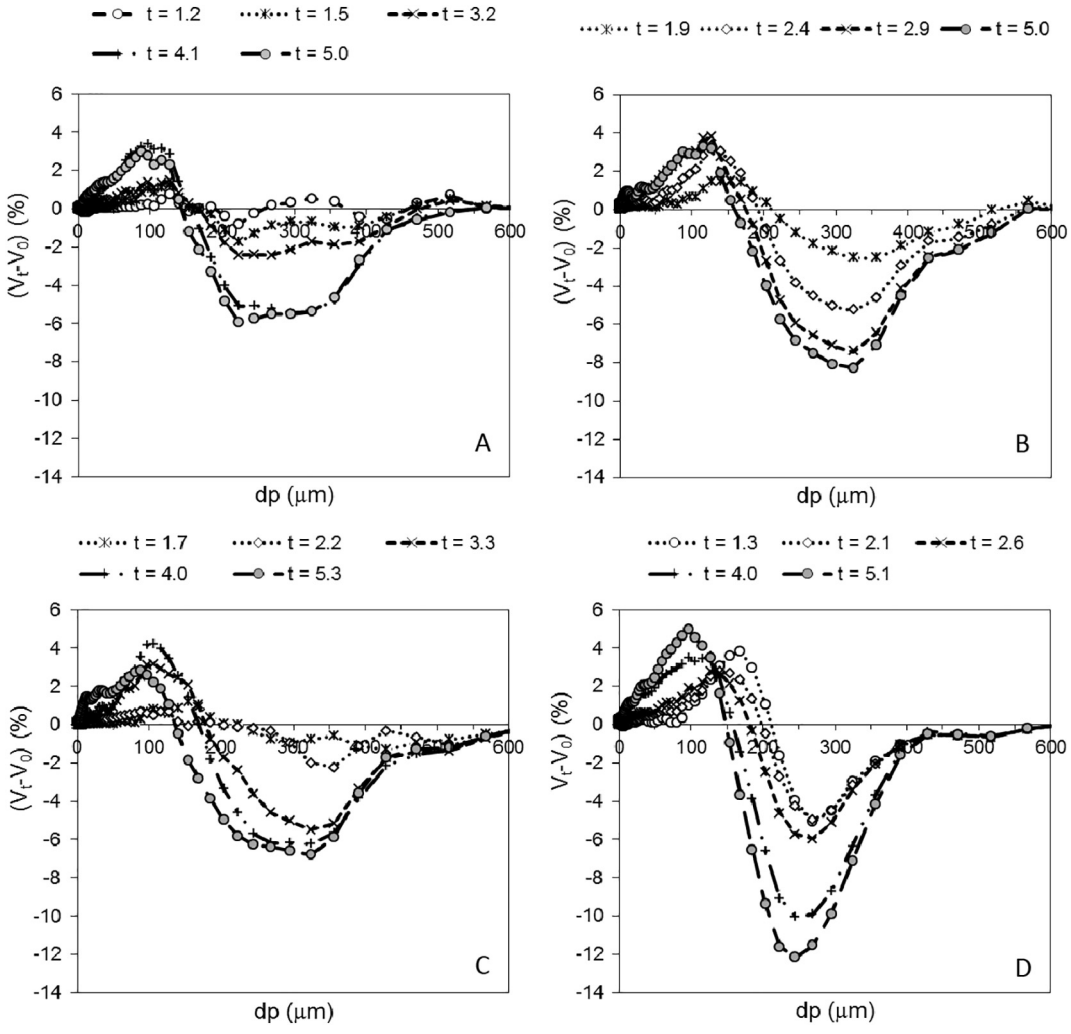

Fig. 7. Sinusoidal-type curves from eq. (6) for all limestones at different experimental times.

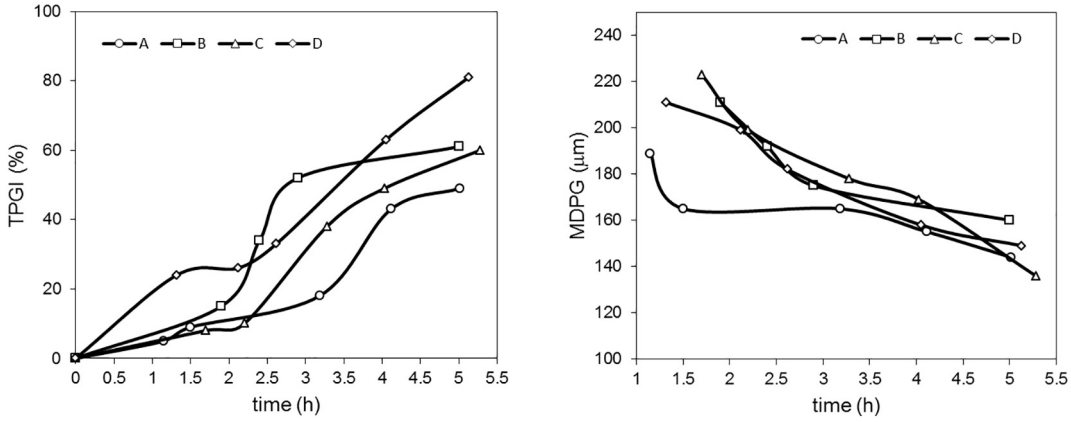

Fig. 8. Evolution with time of TPGI (Left) and MDPG (Right) for all limestones in the 30 kW pilot plant.

Fig. 4 are those proposed by Amblard et al. [39], as the TPGI takes into account the changes in the entire PSD, whereas the MDPG is useful for deducing the main attrition mechanism.

4. Conclusions

The resistance to attrition of four commercial limestones with similar chemical composition has been studied in a 30 kWth fluidized-bed pilot plant operated under conditions similar to those in larger calcium looping systems. The study of the evolution of the particle size distributions with time allowed the main attrition mechanisms for each limestone to be identified. During a first heating up period before calcination, with intense solid circulation, fragmentation of limestone was clearly observed in three out of four of the limestones used in this study. During the period of maximum calcination rates, decrepitation mechanism promoted the attrition of all the limestones tested, but in very different degrees. Abrasion of CaO particles after calcination was also detected by monitoring the evolution of PSDs curves with time, and it was possible to identify one of the solids very resistant to this type of attrition mechanism. The experimental data obtained from the pilot plant tests were used to calculate and compare attrition indexes reported in the literature for characterizing the limestones according to their mechanical strength during the fluidization at high temperature. Neither the Attrition Index defined by Gwyn nor that proposed by Forsythe and Hertwig are able to account sufficiently well for the changes observed in the PSD curves. However, the Total Particle Generated Index (TPGI) and the maximum particle size generated (MDPG) during attrition, which require the re-construction of the PSDs of the elutriated and non-elutriated solids, gave a more accurate description of the attrition phenomena With this methodology, it is possible to distinguish different attrition mechanisms and rank the materials.

Acknowledgments

This research was partially funded by the European Community Research Fund for Coal and Steel (CaO2 project: RFC-PR-13006) and from the Spanish Ministry of Economy and Competitivity ENE2015-68885-C2-1-R.

References

[1] T. Shimizu, T. Hirama, H. Hosoda, K. Kitano, M. Inagaki, K. Tejima, A twin fluid-bed reactor for removal of CO_2 from combustion processes, Chem. Eng. Res. Des. 77 (1999) 62–68.
[2] J.C. Abanades, B. Arias, A. Lyngfelt, T. Mattisson, D.E. Wiley, H. Li, M.T. Ho, E. Mangano, S. Brandani, Emerging CO_2 capture systems, Int. J. Green. Gas. Cont. 40 (2015) 126–166.
[3] D.P. Hanak, E.J. Anthony, V. Manovic, A review of developments in pilot-plant testing and modelling of calcium looping process for CO_2 capture from power generation systems, Energy Environ. Sci. 8 (2015) 2199–2249.
[4] M.E. Boot-Handford, J.C. Abanades, E.J. Anthony, M.J. Blunt, S. Brandani, N. Mac Dowell, J.R. Fernández, M.C. Ferrari, R. Gross, J.P. Hallett, R.S. Haszeldine, P. Heptonstall, A. Lyngfelt, Z. Makuch, E. Mangano, R.T.J. Porter, M. Pourkashanian, G. T. Rochelle, N. Shah, J.G. Yao, P.S. Fennell, Carbon capture and storage update, Energy Environ. Sci. 7 (2014) 130–189.
[5] J.C. Abanades, Calcium looping for CO_2 capture in combustion systems, in: F. Scala (Ed.), Fluidized Bed Technologies for near-zero Emission Combustion and Gasification, Woodhead Publishing Limited, Cambridge 2013, pp. 931–971.
[6] C.C. Dean, J. Blamey, N.H. Florin, M.J. Al-Jeboory, P.S. Fennell, The calcium looping cycle for CO_2 capture from power generation, cement manufacture and hydrogen production, Chem. Eng. Res. Des. 89 (2011) 836–855.
[7] J. Blamey, E.J. Anthony, J. Wang, P.S. Fennell, The calcium looping cycle for large-scale CO_2 capture, Prog. Energy Comb. Sci. 36 (2010) 260–279.
[8] B. Arias, M.E. Diego, J.C. Abanades, M. Lorenzo, L. Diaz, D. Martínez, J. Alvarez, A. Sánchez-Biezma, Demonstration of steady state CO_2 capture in a 1.7MWth calcium looping pilot, Int. J. Green. Gas. Cont. 18 (2013) 237–245.
[9] J. Ströhle, M. Junk, J. Kremer, A. Galloy, B. Epple, Carbonate looping experiments in a 1 MWth pilot plant and model validation, Fuel 127 (2014) 13–22.
[10] H. Dieter, C. Hawthorne, M. Zieba, G. Scheffknecht, Progress in Calcium Looping post combustion CO_2 Capture: Successful pilot scale demonstration, Energy Procedia 2013, pp. 48–56.
[11] M. Alonso, M.E. Diego, J.C. Abanades, C. Perez, J. Chamberlain, Biomass combustion with in situ CO_2 capture by CaO in a 300 kW_{th} circulating fluidized bed test facility, Int. J. Green. Gas. Cont. 29 (2014) 142–152.
[12] M.H. Chang, C.M. Huang, W.H. Liu, W.C. Chen, J.Y. Cheng, W. Chen, T.W. Wen, S. Ouyang, C.H. Shen, H.W. Hsu, Design and experimental investigation of calcium looping process for 3-kWth and 1.9-MWth facilities, Chem. Eng. Technol. 36 (2013) 1525–1532.
[13] C.R. Bemrose, J. Bridgwater, A review on attrition and attrition test methods, Powder Technol. 49 (1987) 97–126.
[14] G.W. Vaux, D.L. Keairns, Attrition in fluid-bed processes, in: J.R. Grace, J.M. Matsen (Eds.),International Fluidization Conference, Plenum, New York 1980, pp. 437–444.
[15] G.W. Vaux, A.W. Fellers, Measurement of attrition tendency in fluidization, AIChE Symp. Ser. 205 (1981) 107–115.
[16] A. Thon, J. Werther, Attrition resistance of a VPO catalyst, Appl. Catal., A 376 (2010) 56–65.
[17] F. Scala, A. Cammarota, R. Chirone, P. Salatino, Comminution of limestone during batch fluidized-bed calcination and Sulfation, AIChE J. 43 (1997) 363–373.
[18] F. Scala, P. Salatino, R. Boerefijn, M. Ghadiri, Attrition of sorbents during fluidized bed calcination and sulphation, Powder Technol. 107 (2000) 153–167.
[19] F. Montagnaro, P. Salatino, F. Scala, The influence of temperature on limestone sulfation and attrition under fluidized bed combustion conditions, Experimental Thermal & Fluid Science 34 (2010) 352–358.
[20] F. Scala, R. Chirone, P. Salatino, Attrition phenomena relevant to fluidized bed combustion and gasification systems, in: F. Scala (Ed.), Fluidized Bed Technologies for near-zero Emission Combustion and Gasification, Woodhead Publishing Limited, Cambrigde 2013, pp. 254–314.
[21] T. Shimizu, M. Peglow, S. Sakuno, N. Misawa, N. Suzuki, H. Ueda, H. Sasatsu, H. Gotou, Effect of attrition on SO_2 capture by limestone under pressurized fluidized bed combustion conditions-comparison between a mathematical model of SO_2 capture by single limestone particle under attrition condition and SO_2 capture in a large-scale PFBC, Chem. Eng. Sci. 56 (2001) 6719–6728.
[22] T. Shimizu, M. Peglow, K. Yamagiwa, M. Tanaka, S. Sakuno, N. Misawa, N. Suzuki, H. Ueda, H. Sasatsu, H. Gotou, A simplified model of SO_2 capture by limestone in 71 MWe pressurized fluidized bed combustor, Chem. Eng. Sci. 57 (2002) 4117–4128.
[23] F. Montagnaro, F. Pallonetto, P. Salatino, F. Scala, Steam reactivation of a spent sorbent for enhanced SO_2 capture in FBC, AIChE J. 52 (2006) 4090–4098.
[24] J.J. Saastamoinen, Particle-size optimization for SO_2 capture by limestone in a circulating fluidized bed, Ind. Eng. Chem. Res. 46 (2007) 7308–7316.
[25] J.J. Saastamoinen, T. Shimizu, Attrition-enhanced sulfur capture by limestone particles in fluidized beds, Ind. Eng. Chem. Res. 46 (2007) 1079–1090.

[26] F. Montagnaro, P. Salatino, F. Scala, R. Chirone, An assessment of water and steam reactivation of a fluidized bed spent sorbent for enhanced SO_2 capture, Powder Technol. 180 (2008) 129–134.
[27] A. Coppola, F. Scala, P. Salatino, F. Montagnaro, Fluidized bed calcium looping cycles for CO_2 capture under oxy-firing calcination conditions: part 1. Assessment of six limestones, Chem. Eng. J. 231 (2013) 537–543.
[28] A. Coppola, F. Montagnaro, P. Salatino, F. Scala, Attrition of limestone during fluidized bed calcium looping cycles for CO_2 capture, Combust. Sci. Technol. 184 (2012) 929–941.
[29] V. Manovic, E.J. Anthony, Lime-based sorbents for high-temperature CO_2 capture-a review of sorbent modification methods, Int. J. Environ. Res. Public Health 7 (2010) 3129–3140.
[30] L. Jia, R. Hughes, D. Lu, E.J. Anthony, I. Lau, Attrition of calcining limestones in circulating fluidized-bed systems, Ind. Eng. Chem. Res. 46 (2007) 5199–5209.
[31] P.S. Fennell, R. Pacciani, J.S. Dennis, J.F. Davidson, A.N. Hayhurst, The effects of repeated cycles of calcination and carbonation on a variety of different limestones, as measured in a hot fluidized bed of sand, Energy Fuel 21 (2007) 2072–2081.
[32] F. Fang, Z.S. Li, N.S. Cai, Continuous CO_2 capture from flue gases using a dual fluidized bed reactor with calcium-based sorbent, Ind. Eng. Chem. Res. 48 (2009) 11140–11147.
[33] B. González, M. Alonso, J.C. Abanades, Sorbent attrition in a carbonation/calcination pilot plant for capturing CO_2 from flue gases, Fuel 89 (2010) 2918–2924.
[34] A. Charitos, C. Hawthorne, A.R. Bidwe, S. Sivalingam, A. Schuster, H. Spliethoff, G. Scheffknecht, Parametric investigation of the calcium looping process for CO2 capture in a 10 kW(th) dual fluidized bed, Int. J. Green. Gas. Cont. 4 (2010) 776–784.
[35] J. Saastamoinen, T. Pikkarainen, A. Tourunen, M. Räsänen, T. Jäntti, Model of fragmentation of limestone particles during thermal shock and calcination in fluidised beds, Powder Technol. 187 (2008) 244–251.
[36] J.J. Saastamoinen, T. Shimizu, A. Tourunen, Effect of attrition on particle size distribution and SO_2 capture in fluidized bed combustion under high CO_2 partial pressure conditions, Chem. Eng. Sci. 65 (2010) 550–555.
[37] W.L. Forsythe, W.R. Hertwig, Attrition characteristics of fluid cracking catalysts, Industrial & Engineering Chemistry 41 (1949) 1200–1206.
[38] J.E. Gwyn, On the particle size distribution function and the attrition of cracking catalysts, AICHE J. 15 (1969) 35–39.
[39] B. Amblard, S. Bertholin, C. Bobin, T. Gauthier, Development of an attrition evaluation method using a jet cup rig, Powder Technol. 274 (2015) 455–465.
[40] M. Alonso, Y.A. Criado, J.C. Abanades, G. Grasa, Undesired effects in the determination of CO_2 carrying capacities of CaO during TG testing, Fuel 127 (2014) 52–61.
[41] G.S. Grasa, J.C. Abanades, CO_2 capture capacity of CaO in long series of carbonation/calcination cycles, Ind. Eng. Chem. Res. 45 (2006) 8846–8851.
[42] M. Alonso, N. Rodriguez, B. González, G. Grasa, R. Murillo, J.C. Abanades, Postcombustion capture of CO_2 with CaO in a circulating fluidized bed carbonator, in: G. Yue, H. Zhang, C. Zhao, Z. Luo (Eds.), 20th Fluidized Bed Combustion, Springer, Xian (China) 2009, pp. 549–554.
[43] M. Alonso, N. Rodriguez, B. Gonzalez, G. Grasa, R. Murillo, J.C. Abanades, Carbon dioxide capture from combustion flue gases with a calcium oxide chemical loop. Experimental results and process development, Int. J. Green. Gas. Cont. 4 (2010) 167–173.
[44] N. Rodriguez, M. Alonso, J.C. Abanades, Experimental investigation of a circulating fluidized-bed reactor to capture CO_2 with CaO, AICHE J. 57 (2011) 1356–1366.